PCCP

Accepted Manuscript

ROYAL SOCIETY OF CHEMISTRY

rsc.li/pccp

View Article Online
DOI: 10.1039/C9CP02389E

Journal Name

ARTICLE TYPE

Cite this: DOI: 10.1039/xxxxxxxxxx

Non-equilibrium thermodynamics as a tool to compute temperature at the catalyst surface

Carolina Cruz,[†a], Daniel Barragán,[*a] Elisa Magnanelli,[b] Anders Lervik,[b] and Signe Kjelstrup[b]

Received Date
Accepted Date

DOI: 10.1039/xxxxxxxxxx

www.rsc.org/journalname

The surface temperature is computed for a heterogeneous catalytic reaction model, namely the oxidation of carbon monoxide on platinum. The surface temperature was found using non-equilibrium thermodynamic theory, a theory which provides the proper dependencies between heat and mass fluxes and the reaction rate. The theory predicts a possible coupling between the reaction rate and the thermal driving force and can help extend classical reaction kinetics. In absence of direct measurements, we explore the coupling numerically. The results are able to capture experimental data reported in the literature, and give new insights into why Arrhenius plots may turn out to be non-linear.

1 Introduction

Heterogeneous catalysis is a well-established field, see e.g.[1] The core of the theoretical modeling in this field corresponds to a set of equations that describes consecutive steps: adsorption of reactants, chemical reaction(s) at the catalytic surface, and desorption. The law-of-mass-action is often used to describe these steps. Usually, the interest is on the conditions that determine the overall reaction rate; this is, for instance, the surface coverage of reactants/products molecules and the surface temperature. Depending on the catalyst structure, the active site is, however, often located inside a pore of a heterogeneous medium. In the case of gases, not only a concentration gradient arises from the bulk stream to the catalytic site, but also a temperature gradient may appear.[2,3] The magnitude of interfacial temperature gradients depends on the nature of processes involved, some representative experimental values are: an interfacial temperature jump close to 0.2K during the crystallization of $MgSO_4$ from aqueous solution and over a cold plate,[4] up to 1.68K at a forming ice-water interface,[5] a maximal of 15.68K across the water-vapor interface during steady-state evaporation a low-pressure and in the presence of vapor phase heating,[6] at least of 20K during the carbon monoxide oxidation over alumina-supported platinum catalyst with microwave heating[7,8] and, a temperature jump close to 1K during biological active transport of calcium in a single HeLa cell.[9]

The chemical reaction is commonly an activated process, and therefore modeled with rate constants that follow Arrhenius' law. For a forward reaction rate with rate coefficient k_f, this may take the form $k_f = k\exp[-E_a/RT]$, where E_a is the activation energy, R is the gas constant, T is the temperature at which the reaction takes place and k is a constant. In order to find the characteristic activation energy E_a, $\ln k_f$ is plotted vs $1/T$, with the expectation that the plot is a straight line. In presence of temperature gradients, it is, however, difficult to know the surface temperature at which the reaction takes place since it can differ from that of the neighboring bulk phase. For instance, a system with an exothermic reaction may have a higher temperature at the catalytic site T^s, where the enthalpy of reaction is released, then at the position of the thermocouple, where the temperature is measured T^g. For a system with an endothermic reaction, the situation may be reversed. A plot of $\ln k_f$ vs $1/T^g$ may then not appear as a straight line, while a plot vs $1/T^s$ would have been.

This problem has been recognized since long.[7,10,11]

[a] Escuela de Química, Facultad de Ciencias, Universidad Nacional de Colombia, Carrera 65 No 59A-110, Medellin, Colombia.
[b] Department of Chemistry, Norwegian University of Science and Technology, NO-7491 Trondheim, Norway.
[†] Present address:Institute of Physical Chemistry, Polish Academy of Sciences, 01-224, Warszawa, Poland
[*] Corresponding author: dalbarraganr@unal.edu.co

View Article Online
DOI: 10.1039/C9CP02389E

Clearly, it is not sufficient to describe this phenomenon using chemical reaction kinetics. The heat flux should be coupled to the mass flux. It is known from studies of phase transitions[12] that the coupling coefficient is large at interfaces. It is not straightforward to mend the situation, but one way to deal with such a coupling is to use non-equilibrium thermodynamics (NET). The framework of this theory was laid out by Bedeaux and coworkers[13,14] for heterogeneous catalysis.

Zhu and Frens[15] proposed that apparent deviations from a linear Arrhenius behavior would disappear using this theory, but they did not take advantage of the theory for more detailed studies of this problem. This is the main topic of this work.

A peculiar property of the NET theory is the prediction that the reaction rate is a function, not only of the well-known driving force (i.e. the negative reaction Gibbs energy of the surface over the surface temperature, $-\Delta_r G^s/T^s$), but also of the difference in the inverse temperature between the surface and the adjacent environment, $\Delta(1/T)$. The prediction has lead to the formulation of a non-isothermal Michaelis-Menten kinetics scheme,[16] and to a description of the Ca^{2+}-ATPase, not only as a pump for Ca^{2+}-ion-transport,[17] but also as heat pump.[18,19] These interesting phenomena serve as inspiration in this case. Our aim is also to bring out in more detail the relation between the chemical reaction rate and its thermal driving force; thereby adding to chemical reaction kinetics.

The Langmuir-Hinselwood set of equations describe a central type of heterogeneous catalysis reactions,[1] where the reacting components are chemisorbed on the surface of the catalyst before the chemical reaction takes place. We shall use an example that follows this pattern to illustrate the theory at work. We shall see that indeed, for an exothermic reaction, the surface temperature is underestimated. A suitable example is the oxidation of carbon monoxide on a platinum crystal. The reaction between carbon monoxide and oxygen has long been the subject of experimental studies and its mechanism and kinetics are well understood.[20,21] In experiments at low surface coverage where the catalyst surface is covered by oxygen, the reaction obeys the Langmuir-Hinshelwood model.[22] The catalytic process begins with adsorption and dissociation of O_2 on the surface, before carbon monoxide is adsorbed:

$$\frac{1}{2}O_2 + Z \rightleftharpoons ZO \quad (1)$$

$$CO + Z \rightleftharpoons ZCO \quad (2)$$

where CO and O_2 are components in the gas phase (non-adsorbed) whereas ZCO and ZO denote adsorbed components, *i.e.* molecule or atom bound to the active site Z.

The oxygen atom and carbon monoxide molecule adsorbed in the surface react then to form CO_2, which is desorbed almost instantaneously, due to its weak interaction with the platinum surface:

$$ZO + ZCO \rightleftharpoons CO_2 + 2Z \quad (3)$$

2 The surface as a system

In the theory of NET of heterogeneous systems, the surface between the gas phase and the solid state catalyst is handled as a separate, *i.e.* autonomous thermodynamic system. The properties are defined following Gibbs' description. The surface thickness, δ^s, is smaller by orders of magnitude than the adjacent gas and catalyst support films which have thicknesses δ^g and δ^c, respectively. Figure 1 represents the three subsystems where the surface is independent, but coupled to the others. The reactants in the bulk gas phase, O_2 and CO, diffuse towards the surface where they react. The reaction product, CO_2, diffuses from the surface back into the gas phase. Reactions take place only at the surface. Only heat can leave the surface through the catalyst. In reality, the solid phase may be in contact with reactor walls, meaning that there is a sink of heat through the catalyst. The mass and heat fluxes are also indicated in the figure. The terms surface and interface will be used interchangeably in this work. They both refer to the catalyst-gas surface layer.

3 Thermodynamic formulation

Thermodynamic properties of the surface are defined following Gibbs' description, and chemical reaction must be described within the same framework, see[14] for details. The adsorption and desorption steps are handled as linearly coupled transport equations, standard for non-equilibrium thermodynamics. We shall use this formalism here, with the example chosen.

We shall address the system in a stationary state. This makes the total heat flux (J_q) and the total mass flux ($J = J_{CO} + J_{O_2} + J_{CO_2}$) constant across the system. Moreover, since there is no mass flow through the catalyst phase, the total mass flux equals zero ($J = 0$). Thermodynamic models for the three subsystems of Fig. 1 follow from this condition.

3.1 Gas phase

The gas phase is a mixture of three components (CO, O_2, and CO_2) which is described by assuming ideal gas law. The entropy production of the homogeneous gas phase

View Article Online
DOI: 10.1039/C9CP02389E

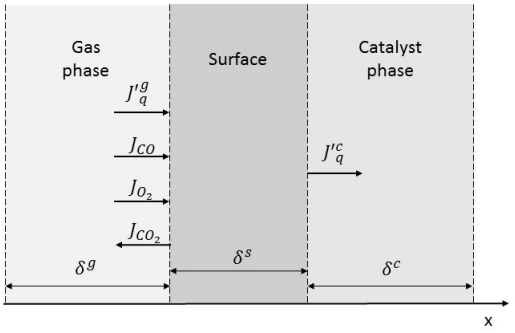

Fig. 1 Schematic representation of a heterogeneous catalytic system in one dimension. The heterogeneous catalytic system is made up by a gas phase (with thickness δ^g), a catalyst solid phase (with thickness δ^c), and a surface that separates them (with thickness δ^s). The subsystems exchange heat and mass. Proportions between the thicknesses of the subsystems are not respected. Mass fluxes of reactants (J_{CO} and J_{O_2}) and product (J_{CO_2}) move across the gas phase in opposite directions. The reaction takes place in the surface. No mass can flow through the catalyst phase, while heat fluxes are present both in the gas and in the catalyst phase (J'^g_q and J'^c_q).

is:[14]

$$\sigma^g = J_q \frac{d}{dx}\left(\frac{1}{T}\right) + J_{CO}\left(-\frac{d}{dx}\frac{\mu_{CO}}{T}\right) + J_{O_2}\left(-\frac{d}{dx}\frac{\mu_{O_2}}{T}\right) + J_{CO_2}\left(-\frac{d}{dx}\frac{\mu_{CO_2}}{T}\right) \quad (4)$$

where σ^g is the entropy production in the gas phase, J_q is the total heat flux, T is the temperature, and μ_j and J_j are the chemical potentials and the mass fluxes of the components $j = \{CO, O_2, CO_2\}$. It is important to note that there is no conservation with respect to the atomic species due to the chemical reaction and, for future calculations, variables are expressed in mass units. The total heat flux can be expressed in terms of measurable heat flux and mass fluxes in the gas phase:

$$J_q = J'^g_q + \sum_j H_j J_j \quad (5)$$

where J'^g_q is the measurable heat flux in the gas phase, and H_j is the component partial enthalpy.

By substituting Eq. 5 into Eq. 4, we obtain:

$$\sigma^g = J'^g_q \frac{d}{dx}\frac{1}{T} + J_{CO}\left(-\frac{d}{dx}\frac{\mu_{CO}}{T} + H_{CO}\frac{d}{dx}\frac{1}{T}\right) + J_{O_2}\left(-\frac{d}{dx}\frac{\mu_{O_2}}{T} + H_{O_2}\frac{d}{dx}\frac{1}{T}\right) + J_{CO_2}\left(-\frac{d}{dx}\frac{\mu_{CO_2}}{T} + H_{CO_2}\frac{d}{dx}\frac{1}{T}\right) \quad (6)$$

For the gas phase, Eq. 6 has both, thermal and chemical driving forces. The relations between driving forces and fluxes in the homogeneous phase are linear, as follows:

$$\frac{d}{dx}\frac{1}{T} = r^g_{qq}J'^g_q + r^g_{q1}J_{CO} + r^g_{q2}J_{O_2} + r^g_{q3}J_{CO_2} \quad (7)$$

$$-\frac{d}{dx}\frac{\mu_{CO}}{T} + H_{CO}\frac{d}{dx}\frac{1}{T} = r^g_{1q}J'^g_q + r^g_{11}J_{CO} + r^g_{12}J_{O_2} + r^g_{13}J_{CO_2} \quad (8)$$

$$-\frac{d}{dx}\frac{\mu_{O_2}}{T} + H_{O_2}\frac{d}{dx}\frac{1}{T} = r^g_{2q}J'^g_q + r^g_{21}J_{CO} + r^g_{22}J_{O_2} + r^g_{23}J_{CO_2} \quad (9)$$

$$-\frac{d}{dx}\frac{\mu_{CO_2}}{T} + H_{CO_2}\frac{d}{dx}\frac{1}{T} = r^g_{3q}J'^g_q + r^g_{31}J_{CO} + r^g_{32}J_{O_2} + r^g_{33}J_{CO_2} \quad (10)$$

In order to describe the system, all transport coefficients in Eqs. 7-10 must be known. The coefficients may depend on state variables like temperature and pressure. We only consider the main coefficients, r^g_{ii}. In principle, cross-coupling coefficients, r^g_{ij}, should also be included. The description of the gas phase would then require 10 independent transport coefficients (the cross-coupling coefficients are related by the Onsager reciprocal relations:[23,24] $r^g_{ij} = r^g_{ji}$). The cross-coupling coefficients are usually smaller than the main transport coefficients in a homogeneous phase.[25,26] Therefore, we neglect these cross-coupling coefficients in the following.

The main transport coefficients can be calculated from the thermal conductivity and the diffusion coefficients of the gas. According to Fourier's and Fick's laws, the measurable heat flux and the mass fluxes are related to thermal conductivity and diffusion coefficients:[27]

$$J'^g_q = -\lambda^g \frac{dT}{dx} \quad (11)$$

$$J_j = -D^g_j \frac{dC_j}{dx} \quad (12)$$

where λ^g is the thermal conductivity of the gas, and D^g_j is the diffusion coefficient of component j. The common frame of reference for all fluxes is the surface. A common choice is needed to use the same mass and energy flux through the system.

By comparing Eqs. 11-12 with Eqs. 7-10 and neglecting the coupling coefficients, the main transport coefficients are calculated:

$$r^g_{qq} = \frac{1}{\lambda^g T^2} \quad (13)$$

$$r^g_{jj} = \frac{1}{D^g_j T}\frac{\partial \mu_j}{\partial C_j}\bigg|_{T=\text{const.}} \quad (14)$$

3.2 Catalyst

The catalyst is a solid material (here a platinum crystal), where only heat can be transported. The entropy production of the catalyst, σ^c, is simply:

$$\sigma^c = J'^c_q \frac{d}{dx}\left(\frac{1}{T}\right) \quad (15)$$

View Article Online
DOI: 10.1039/C9CP02389E

where $J_q'^c$ is the measurable heat flux in the catalyst phase. The force-flux relation for this subsystem is:

$$\frac{d}{dx}\left(\frac{1}{T}\right) = r_{qq}^{c} J_q'^c \tag{16}$$

Here the heat transport coefficient, r_{qq}^{c}, can be calculated as:

$$r_{qq}^{c} = \frac{1}{\lambda^c T^2} \tag{17}$$

where λ^c is the thermal conductivity of the catalyst material.

3.3 Surface

The entropy production at the surface is an excess property,[14] integrated out over the thickness of the surface, leading to discrete formulations of the driving forces in the entropy production:

$$\begin{aligned}\sigma^s = {} & J_q'^s\left(\frac{1}{T^s}-\frac{1}{T^g}\right)+J_q'^c\left(\frac{1}{T^c}-\frac{1}{T^s}\right)\\ & + J_{CO}\left[-\left(\frac{\mu_{CO}^s}{T^s}-\frac{\mu_{CO}^g}{T^g}\right)+H_{CO}^g\left(\frac{1}{T^s}-\frac{1}{T^g}\right)\right]\\ & + J_{O_2}\left[-\left(\frac{\mu_{O_2}^s}{T^s}-\frac{\mu_{O_2}^g}{T^g}\right)+H_{O_2}^g\left(\frac{1}{T^s}-\frac{1}{T^g}\right)\right]\\ & + v^s\left(-\frac{1}{T^s}\Delta_r G^s\right)\end{aligned} \tag{18}$$

where $\Delta_r G^s$ is the reaction Gibbs energy. The last term of Eq. 18 describes the reaction, while the second and third terms describe the adsorption. Surface properties are referred to using the superscript "s". Superscripts "g" and "c" are used for the gas phase and catalyst, respectively.

The symbol v^s denotes the reaction rate. For isothermal conditions, with equilibrium between the surface and the gas, it is given by the law of mass action:[20,28,29]

$$v^s = \delta^s\left(k_f C_{COZ}^s C_{OZ}^s - k_b C_{CO_2}^s C_Z^{s\,2}\right) \tag{19}$$

where k_f ands k_b are kinetic constants for the forward and the backward reaction in Eq. 3. Here, C_j^s is the molar density at the surface of component j and it is calculated following a Langmuir-Hinshelwoods kinetics[1], where equilibrium constants for adsorption of oxygen and carbon monoxide, K_{CO} and K_{O_2}, are needed. The reaction constants k_f and k_b are given by the Arrhenius expression:

$$k_f = k_{0,f}\exp\left(\frac{-E_{a,f}}{RT}\right) \tag{20}$$

$$k_b = k_{0,b}\exp\left(\frac{-E_{a,b}}{RT}\right) \tag{21}$$

where $k_{0,f}$ and $k_{0,b}$ are the pre-exponential factors, and $E_{a,f}$ and $E_{a,b}$ are the activation energies.

The force-flux relations at the surface are:[14]

$$\left(\frac{1}{T^s}-\frac{1}{T^g}\right) = r_{qq}^{s,g} J_q'^g + r_{q1}^{s,g} J_{CO} + r_{q2}^{s,g} J_{O_2} + r_{qr}^{s,g} v^s \tag{22}$$

$$\left(\frac{1}{T^c}-\frac{1}{T^s}\right) = r_{qq}^{s,c} J_q'^c \tag{23}$$

$$-\left(\frac{\mu_{CO}^s}{T^s}-\frac{\mu_{CO}^g}{T^g}\right)+H_{CO}^g\left(\frac{1}{T^s}-\frac{1}{T^g}\right) = r_{q1}^{s,g} J_q'^g + r_{11}^{s,g} J_{CO} \tag{24}$$

$$-\left(\frac{\mu_{O_2}^s}{T^s}-\frac{\mu_{O_2}^g}{T^g}\right)+H_{O_2}^g\left(\frac{1}{T^s}-\frac{1}{T^g}\right) = r_{q2}^{s,g} J_q'^g + r_{22}^{s,g} J_{O_2} \tag{25}$$

$$\left[1-\exp\left(\frac{\Delta_r G^s}{RT^s}\right)\right] = r_{rq}^{s,g} J_q'^g + r_{rr}^{s,g} v^s \tag{26}$$

where $r_{ji}^{s,g}$ and $r_{ji}^{s,c}$ are the transport coefficients of the surface, which have the units of the transport coefficients for an homogeneous phase times a length. From Eqs. 7-10 most of the coupling coefficients related to mass fluxes have been neglected. We have left the coefficients related to the heat flux and obtained Eqs. 22-26.

The force-flux relation (Eq. 26) between the reaction driving force, $-\Delta_r G^s/T^s$, and the flux is not linear[30] on this level of description. It results from integration over an internal coordinate, the degree of reaction, with a linear flux-force relation. We refer to[30] for details.

No experimental data are available for the heat transport coefficients of the selected surface. However, experimental data on other interfaces show that, in comparison to its thickness, the surface has a higher resistance to transport than its neighboring homogeneous phases.[31,32] Thus, we consider that the heat transfer coefficients can be estimated starting from those of the neighboring homogeneous phases as:[25]

$$r_{qq}^{s,g} = \beta\,\delta^s r_{qq}^{g} \tag{27}$$

$$r_{qq}^{s,c} = \beta\,\delta^s r_{qq}^{c} \tag{28}$$

where $\beta > 1$ is a scaling factor.

The main mass transport coefficients are estimated from the adsorption rates of CO and O_2 into the surface. The mass fluxes into the surface are written as:

$$J_{CO} = \nu_{CO} = \delta^s\left(k_1 C_{CO} C_Z - k_{-1} C_{COZ}\right) \tag{29}$$

$$J_{O_2} = \nu_{O_2} = \delta^s\left(k_2 C_{O_2}^{1/2} C_Z - k_{-2} C_{OZ}\right) \tag{30}$$

where ν_{CO} and ν_{O_2} are the net reaction rates of adsorption, k_1 and k_2 are the forward constants, and k_{-1} and k_{-2} are the backward constants of the reactions given by Eqs. 1 and 2. By comparing

View Article Online
DOI: 10.1039/C9CP02389E

Eqs. 24 and 25 with Eqs. 29 and 30, we get:

$$r_{11}^{s,g} = -\frac{1}{\nu_{CO}} \frac{\Delta G_{CO}^{s,g}\big|_{J_q'^g=0}}{T} \tag{31}$$

$$r_{22}^{s,g} = -\frac{1}{\nu_{O_2}} \frac{\Delta G_{O_2}^{s,g}\big|_{J_q'^g=0}}{T} \tag{32}$$

where $\Delta G_j^{s,g}$ is the adsorption (or desorption) Gibbs energy of component j in the catalyst surface.

The coupling coefficients between heat and mass transport can be calculated from the heat of transfer[30] and the resistivity to heat transfer:

$$r_{qj}^{s,g} = -r_{qq}^{s,g} q_j^* \tag{33}$$

where q_j^* is the heat of transfer, which can be estimated as a fraction of the enthalpy change:

$$q_j^* = \left(\frac{J_q'}{J_j}\right)^g_{\Delta T=0} = -\kappa \Delta H_j^{s,g} \tag{34}$$

where $\Delta H_j^{s,g}$ is the heat of adsorption of component j at the catalyst surface, and $0 \leq \kappa \leq 1$ is a scaling factor.

The reaction coefficient can be calculated by using Eq. 19 and Eq. 26 for the case when $J_q'^g = 0$:

$$r_{rr}^{s,g} = \frac{1}{\nu^s}\left[1 - \exp\left(\frac{\Delta_r G^s}{RT^s}\right)\right] \tag{35}$$

The coupling coefficient between heat transfer and the chemical reaction, $r_{rq}^{s,g}$, is related to the capacity of the surface to store heat. By considering that the entropy production is always non-negative, we obtain:

$$\left(r_{rq}^{s,g}\right)^2 \leq r_{qq}^{s,g}\, r_{rr}^{s,g} \tag{36}$$

This criterion is used to check whether the sets of coefficients are thermodynamically feasible or not.

Equation 36 can be rewritten to give a practical way to estimate the surface coupling coefficient:

$$r_{rq}^{s,g} = \sqrt{\alpha\, r_{qq}^{s,g} r_{rr}^{s,g}} \tag{37}$$

where $0 \leq \alpha \leq 1$ is a scaling factor.

4 Numerical simulations

4.1 Solution procedure

The set of equations describing the system was solved by means of computational methods using MATLAB® software.[33] In the calculations, the three sub-systems (gas phase, catalyst and interface) were solved simultaneously. The steady state condition was used, with the total heat and mass fluxes constant across the system. The solution was obtained using an iterative procedure. First, the values of the heat fluxes $J_q'^g$, $J_q'^c$, and mass fluxes J_j were guessed and the later ones are given in Table 1 (see Figure. 1)

Table 1 Guessed mass fluxes

Flux	Value	Units
J_{CO}	5.0×10^{-11}	kg m^{-2} s^{-1}
J_{O_2}	2.9×10^{-11}	kg m^{-2} s^{-1}
J_{CO_2}	-7.5×10^{-11}	kg m^{-2} s^{-1}

Then, Eqs. 7–10 and Eq. 16 were integrated, making use of the guessed fluxes. The integration was carried out using the MATLAB® `ode15s` routine, which is a variable-step, variable-order solver that enables us to solve sets of ordinary differential equations[34]. The procedure was repeated until agreement was obtained with the operation conditions at the boundaries of the system. Iterations were repeated using the `fsolve` solver. In order to integrate the equations, we specified the inlet temperature (T^g) and initial concentrations of the components ($C_{0,CO}$, C_{0,O_2}, and C_{0,CO_2}) at $x = 0$ as a boundary conditions.

4.2 Input data

Table 2 reports the parameters used in the numerical solutions. In order to keep calculations at a reasonable level of complexity, we assumed that the forward reaction constant for the adsorption processes can be written as:

$$k_1 = k_{CO} p_{CO} \tag{38}$$

$$k_2 = k_{O_2} p_{O_2} \tag{39}$$

where k_{CO} and k_{O_2} denote the rate at which the gases hit the surface per unit pressure, and p_{CO} and p_{O_2} are the partial pressures of the component in the gas. The recombinative desorption of adsorbed oxygen was neglected (k_{-2}=0), while the backward constant of carbon monoxide follows an Arrhenius-kind of expression:[20]

$$k_{-1} = k_{0,CO} \exp\left(\frac{-E_{a,CO}}{RT}\right) \tag{40}$$

The diffusion coefficients of the components in the gas phase were estimated by using the Fuller correlation.[40] The thermal conductivity of gas phase and catalyst were approximated to the one of carbon monoxide and platinum crystal, respectively. The pressure in the system was kept constant at 1 bar. The nomenclature, symbols and units used in the set of equations are presented in the Appendix 7 and the relevant data for all the parameters and system properties are listed in Table 2.

4.3 Studied cases

In order to analyze the special features of NET formalism compared to standard reaction kinetics description, we proposed three cases. In all cases, we modeled transport in the gas phase with simple transport equations, and the three cases were designed with increasing complexity, as follows:

Case 1: Main coefficients

This case resembles the standard reaction kinetics approaches. In the modeling of the catalytic process, only the main coefficients

View Article Online
DOI: 10.1039/C9CP02389E

addressing the gas film and surface are taken into account. The scaling factor for the main coefficients, β, was varied between 10^2 and 10^7 while κ and α were kept equal to zero.

Case 2: Main and coupling coefficients

For this case, a partially coupled model was considered. Thus, coupling coefficients for mass and heat transfer were added to Case 1. The scaling factors β and κ are varied from 10^2 to 10^7 and 0 to 1, respectively. Here, the scaling factor α was kept equal to zero.

Case 3: Full set of coefficients

In this case, the full set of coefficients were considered: (a) main coefficients of the gas film and surface, (b) at the surface, coupling coefficients of mass and heat transport, and coupling coefficients of reaction and heat transport. Case 3 includes the full coupling between heat transport, mass transport and the chemical reaction, in the sense defined in Section 3. The scaling factors β, κ and α were set to constant values, obtained by fitting the model to experimental results. A sensitivity analysis of these choices were next carried out.

4.4 Transport coefficients

The expressions in Section 3, which were used to compute the transport coefficients, are summarized in Appendix A. The main coefficients for the gas film at $T^{\mathrm{g}} = 500$ K[41], reported in table 3; are all positive, in agreement with the Second Law. The coefficients in this Table are used in cases 1-3.

Table 3 Main transport coefficients of the gas film, at $T^{\mathrm{g}} = 500$ K, $\kappa = 1$, $\alpha = 0.9$, and inlet mole fraction of the gases

Coefficient	Value	Units
r^{g}_{qq}	1.7×10^{-4}	m s J^{-1} K^{-1}
r^{g}_{11}	2.2×10^{13}	J s m K^{-1} kg^{-2}
r^{g}_{22}	2.0×10^{13}	J s m K^{-1} kg^{-2}
r^{g}_{33}	2.0×10^{13}	J s m K^{-1} kg^{-2}

Table B.2 presents all the coefficients of the surface at initial gas temperature, $T^{\mathrm{g}} = 500$ K, and inlet mass fraction of the gases. In section 3 we proposed that the main coefficients at the surface are related to those for the gas film by the scaling factor β, and the surface coupling coefficients and surface main coefficients are related through factors α and κ. The values in table B.2 therefore depend on these parameters. A sensitivity analysis was carried out, keeping in mind that our aim is to evaluate the surface temperature, c.f. Figures. 4– 6. Learning from this sensitivity analysis, we settled on the following set of values: $\beta = 10^6$, $\kappa = 1$ and $\alpha = 0.9$. This set of coefficient are used to define the fully coupled studied case (case 3).

Table 4 Main and coupling coefficients of the surface at $T^{\mathrm{g}} = 500$ K, and inlet mass fraction of the gases. The scaling factors are $\beta = 10^6$, $\kappa = 1$ and $\alpha = 0.9$.

Coefficient	Value	Unit
$r^{s,g}_{qq}$	1.7×10^{-7}	m^2 s J^{-1} K^{-1}
$r^{s,c}_{qq}$	5.6×10^{-11}	m^2 s J^{-1} K^{-1}
$r^{s,g}_{q1}$	3.6×10^{-1}	m^2 s kg^{-1}
$r^{s,g}_{q2}$	1.0×10^{-4}	m^2 s kg^{-1}
$r^{s,g}_{11}$	2.2×10^{11}	J s m^2 K^{-1} kg^{-2}
$r^{s,g}_{22}$	2.0×10^{11}	J s m^2 K^{-1} kg^{-2}
$r^{s,g}_{rq}$	1.4×10^{6}	m^2 W^{-1}
$r^{s,g}_{rr}$	4.3×10^{19}	s kg$_{\mathrm{cat}}$ kg$^{-1}_{\mathrm{CO}}$

5 Results and Discussion

The results of the simulations are reported for Cases 1-3 in Figure 2. Next, we present the temperature profile in the gas phase in Figure 3 for a given set of scaling factors, which we consider to be reasonable. We continue with the sensitivity analysis for scaling factors in Figures 4–6. The main findings are presented in Figures 7 and 8.

5.1 Surface temperature rise above the bulk gas. Studied cases 1-3.

From the set coefficients calculated in the studied cases, we analyze how the surface and gas temperatures depend on the catalytic process. Figure 2 shows the difference between the surface temperature and the bulk gas temperature at various initial gas temperatures, T^{g}, in cases 1-3. The dependence of the surface temperature on the scaling factors is complex, thus we show the results for a selected set of factors (see Sections 5.3 and 5.4) in Figure 2. In the Case 1, it is clear that the exponent, a, of the scaling factor β must be greater than five, in order to see a significant rise in surface temperature above the gas film temperature. For instance, with $\beta = 10^6$ and $T^{\mathrm{g}} = 500$ K, the difference $T^{\mathrm{s}} - T^{\mathrm{g}}$ is less than 5 K, see Figure 2-(a). This means that this case is unable to explain any sizable differences in temperature between the catalytic site and the surroundings.

In Case 2, the temperature difference between the gas and surface increases by considering the contribution of mass-heat coupling coefficients (see Figure 2-(b)). At $T^{\mathrm{g}} = 500$ K and $\kappa = 1$, $T^{\mathrm{s}} - T^{\mathrm{g}}$ is greater than 5 K.

When all coupling coefficients are taken along (Case 3), Figure 2-(c) shows that the temperature difference, $T^{\mathrm{s}} - T^{\mathrm{g}}$, does not change respect Case 2 when the coupling coefficient between heat and mass transport is considered. For this case, we have set the scaling factors equal to $\beta = 10^6$, $\kappa = 1$ and $\alpha = 0.9$, based on experimental results analysis (see Sections 5.3 and 5.4). This means that the predictions made by NET theory seem plausible. We shall consider more aspects of the model below, which strengthens this view.

View Article Online
DOI: 10.1039/C9CP02389E

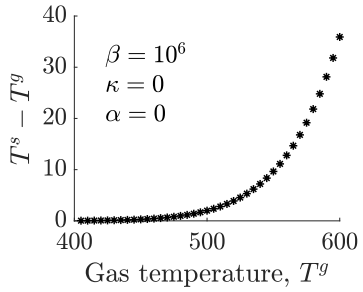

(a) Case 1

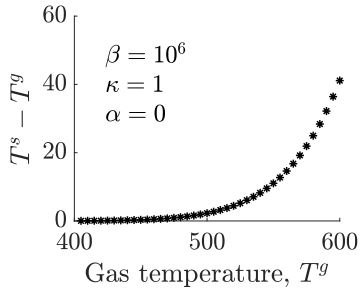

(b) Case 2

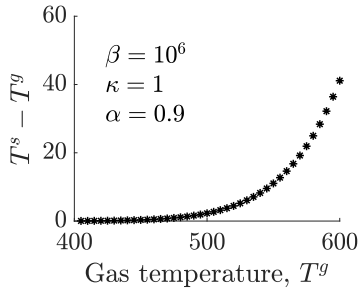

(c) Case 3

Fig. 2 Computed temperature difference, $T^{\mathrm{s}} - T^{\mathrm{g}}$, as a function of T^{g} for the three case studies defined by the scaling factors between the transport coefficients: (a) Case 1, $\beta = 10^6$, $\kappa = 0$ and $\alpha = 0$; (b) Case 2, $\beta = 10^6$, $\kappa = 1$ and $\alpha = 0$; (c) Case 3, $\beta = 10^6$, $\kappa = 1$ and $\alpha = 0.9$

5.2 Gas film temperature profile

In order to achieve a deeper insight into the reason why Case 1 fails for describing a temperature increase, we consider the whole system at steady state. The total heat flux and mass fluxes are constant across the films surrounding the catalyst surface. The two reactants at the inlet have the same concentration, see Table 2.

Figure 3 shows the corresponding temperature profile across the film and surface. The slope in the film is small, and the surface sticks out as a singularity. This is due to the conditions given by the equations of the surface represented as a temperature jump of few degrees at the surface (see the $*$ symbol in Figure 3), and can be ascribed to the enthalpy delivered by the reaction to the surface, where a hold-up of heat is feasible due to the special resistivities. A sensitivity analysis of this result is presented in the next paragraph.

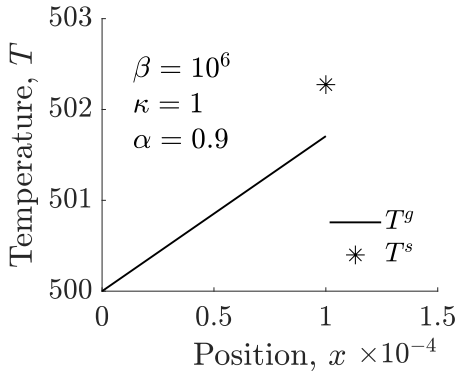

Fig. 3 Spatial temperature profile in the gas film at $T^{\mathrm{g}} = 500$ K. Position is in meters and Temperature in Kelvin. The scaling factors are set equal to $\beta = 10^6$, $\kappa = 1$ and $\alpha = 0.9$. The symbol corresponds to the surface temperature, T^s.

5.3 Estimating scaling factor β from experiments

The surface is assumed to possess a higher resistance to transport compared to the gas phase,[25] meaning that heat flows only through the gas phase. The surface resistivities were obtained by scaling the gas resistivities by a factor β as given in Eq. 27 and 28 which makes the coefficients explicit functions of β. The surface temperature, therefore, has a strong dependency on this factor, and the effect of the surface can be studied directly. The factor depends on the interface nature, for instance, $\beta = 100$ was proposed for a membrane as an interface at a certain temperature,[25] however in this work, the system includes a solid interface, thus another value may be more appropriate. According to Zhu *et al.*,[42] the surface temperature for catalytic hydrogen oxidation differed by at least 34 K from the temperature in the layer before the surface. We build on this experience and propose the following expression for β:

$$\beta = 10^a \tag{41}$$

where $a = 2$ is related to membranes and $a > 3$ can describe solid interfaces. The resulting temperature difference, $\Delta T = T^{\mathrm{s}} - T^{\mathrm{g}}$, is shown as a function of $\beta = 10^a$ in Figure 4 at two different inlet temperatures, T^{g}. We see that β varies with respect to the inlet temperature, and to obtain simulation results that can explain the data in Zhu *et al.*, β must be 10^a with $a > 5$.

5.4 Estimating scaling factor κ: Coupling of heat and mass transport

The parameter κ determines the relation of the coupling between the transport coefficients of heat and mass, *i.e.* the resistivity to heat transfer and the heat of transfer. The meaning of κ in Eq. 34, is simple; it expresses the fraction of the enthalpy for the phase change, or reaction, that leaves the system in the negative direction of transport; *i.e.* goes back to the gas phase. If $\kappa = 1$, all heat enters or leaves by the gas phase; if $\kappa = 0$, all heat leaves

View Article Online
DOI: 10.1039/C9CP02389E

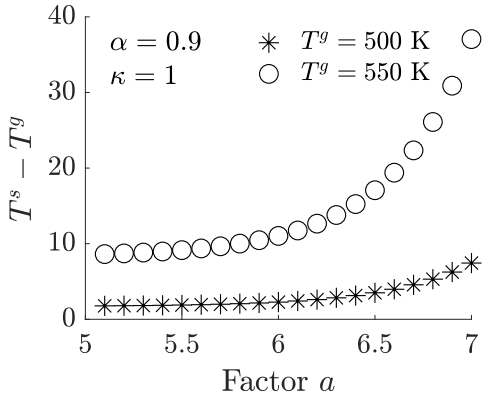

Fig. 4 Surface temperature difference, $\Delta T = T^{\mathrm{s}} - T^{\mathrm{g}}$, as a function of the inlet temperature T^{g} and the scaling factor β. The horizontal axis gives the a-value in the expression $\beta = 10^a$, which varies from 5 to 7. The vertical axis gives the value of ΔT at two different gas temperatures T^g: ($*$) 500 K, and ($\circ$) 550 K. The system is in steady state. The results are obtained using sets of parameters in tables 2–B.2. The scaling factors κ and α are set equal to 1 and 0.9, respectively.

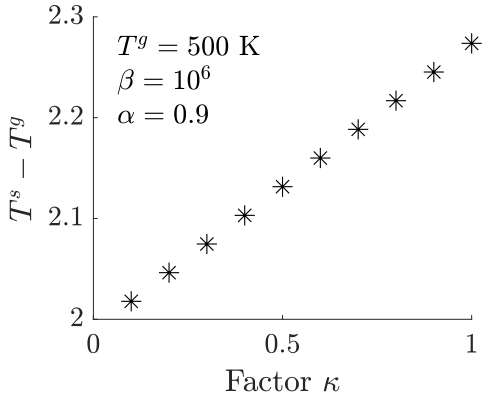

Fig. 5 Surface temperature difference, $T^{\mathrm{s}} - T^{\mathrm{g}}$, obtained with heat and mass coupling coefficients at $T^{\mathrm{g}} = 500$ K, $\beta = 10^6$ and $\alpha = 0.9$. The horizontal axis gives the values of κ. The vertical axis is the surface temperature difference.

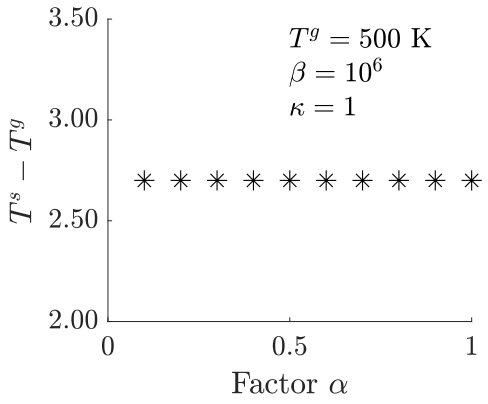

Fig. 6 Surface temperature difference, $T^{\mathrm{s}} - T^{\mathrm{g}}$, from a varying coupling coefficient with $T^{\mathrm{g}} = 500$ K, $\beta = 10^6$ and $\kappa = 1$. The horizontal axis corresponds to the values of the α factor. The vertical axis is the surface temperature difference.

through the catalyst to the reactor wall. Correspondingly for the coupling coefficients (see Eqs. 33 and 34): $\kappa = 0 \implies r^{s,g}_{\mathrm{q}j} = 0$ and $\kappa = 1 \implies r^{s,g}_{\mathrm{q}j} = r^{s,g}_{\mathrm{qq}} \Delta H_j$. Figure 5 represents the surface temperature computed by varying factor κ, *i.e.* varying heat and mass coupling coefficients at $T^{\mathrm{g}} = 500$ K. The effect of this coupling is such there a linear increase in surface temperature at increasing κ. The heat and mass coupling is related to reversible processes; heat carried along by the component.

5.5 Estimating scaling factor α: Coupling of heat transport and reaction

Figure 6 represents the temperature difference by varying factor α, *i.e.* varying heat transport and reaction coupling at the conditions $T^{\mathrm{g}} = 500$ K, $\beta = 10^6$ and $\kappa = 1$. There is no significant influence of the coupling coefficient between heat transfer and reaction on the temperature difference, and this behaviour is consistent with Figs. 2 (a)-(b) since the temperature difference increases by increasing values of β and κ. In Fig. 2 (c), however, the temperature difference does not change by fixing $\kappa = 0.9$.

5.6 Surface temperature and Arrhenius plot

We are now in position to comment on the interesting analysis of experimental data for this system, done by Zhu and Frens.[15] They analyzed the rate of reaction as a function of temperature in the measurement, in order to obtain evidence for a surface temperature being different from that of the measurement or the near surroundings. They suggested to linearize a curved Arrhenius plot to fit the experimental results. Doing this, the measured temperature could be use to estimate surface temperature. Now, in Figure 7 we present the Arrhenius plot obtained from our thermodynamic model. We calculated the reaction rate of the oxidation of carbon monoxide and the temperature at the surface for given values of T^{g}. The figure shows (see the curve with asterisks) that there is no good linear correlation between $\ln \nu^{\mathrm{s}}$ and $1/T^{\mathrm{g}}$. However, when $\ln \nu^{\mathrm{s}}$ is plotted against $1/T^{\mathrm{s}}$ (see the curve with rhombuses), a linear correlation seems reasonable. In other words, our results give quantitative support to the results of Zhu and Frens.[15] The results are interesting, because they support the importance of a special surface temperature, in the analysis of the kinetics of heterogeneous catalytic processes. They defend that there is a benefit by using a more sophisticated theory for the modelling of the events.

5.7 Entropy production in the gas phase and at the surface

The entropy production in a system is a measure of the dissipation of energy, or the irreversibility of the processes.The NET formalism is a tool not only to describe a certain process but also to

View Article Online
DOI: 10.1039/C9CP02389E

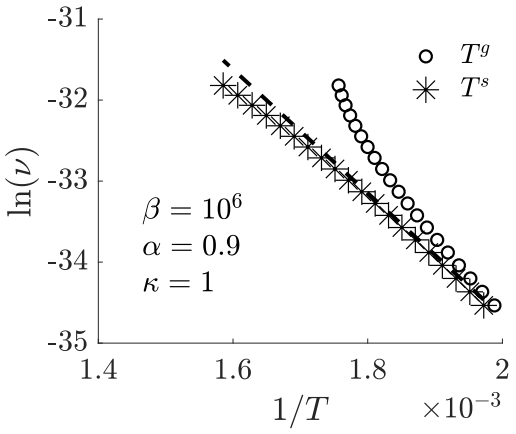

Fig. 7 Computed Arrhenius curve for carbon monoxide oxidation. Circles correspond to T^{g}, and stars correspond to T^{s}. The dashed line represents the linear Arrhenius' equation. The scaling factors are set equal to $\beta = 10^6$, $\kappa = 1$ and $\alpha = 0.9$.

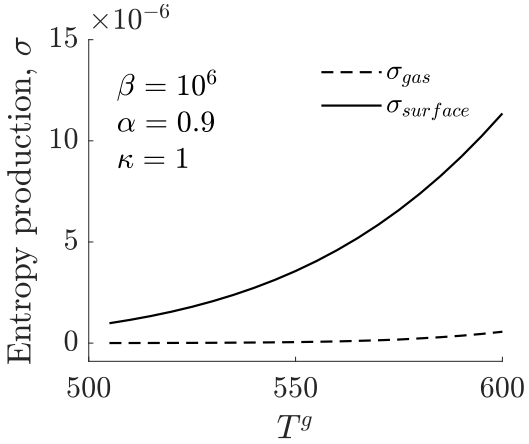

Fig. 8 Calculated entropy production for the heterogeneous catalytic oxidation of carbon monoxide. Curves are obtained at different initial temperatures T^{g} and for the following values of parameters: $E_{\mathrm{a,f}} = 72$ kJ/mol, $\kappa = 1$, $\alpha = 0.9$ and $\beta = 10^6$.

optimize processes that include chemical reactions in a heterogeneous medium.[43] A process can be considered as optimal when its entropy production is minimal. A first step in the direction of minimization, using optimal control theory,[30,43] is to map the location where dissipation takes place. The results in Figure 8 show that the entropy production depends on the nature of chemical reaction and other parameters. There is a higher entropy production at the surface compared to the gas phase as T^g increases. This is consistent since the chemical reaction takes place on the catalyst surface. The art of process optimization seems to be to make this dissipation as uniform as possible.[30,43]

6 Conclusions

We have used NET formalism to describe a heterogeneous catalytic system, exemplified by the Langmuir-Hinselwood type of reaction, and demonstrated how it can be used to examine conditions around the catalytic surface in more details compared to the standard chemical kinetics approach. A simplified kinetic scheme was used to simulate adsorption, reaction and desorption at the catalytic surface, using transport coefficients that were calibrated with experimental values reported in the literature for a particular reaction, the oxidation of carbon monoxide.

The thermodynamic model was set up to include not only coupling between heat and mass fluxes, but also the coupling between reaction rate and heat flux. This is not common in the field of reaction kinetics. We have seen that a reasonable choice of coupling coefficients may influence significantly the conditions at and around the surface. The theory offers, therefore, another way to design experiments that allow us to measure transport coefficients. In particular, reliable regimes of validity and actual values should be established for the scaling factors, β, κ and α, although, this is not a straightforward procedure. In the case of being verified, we believe that our results can contribute to an increased understanding and therefore facing of these important processes.

At this stage, our model supports the analysis of Zhu and Frens,[15] in which the surface temperature can differ from the temperature in the near surroundings by some ten's of degrees. This observation can be used to explain apparent non-linear behavior in Arrhenius plots.

Conflicts of interest

There are no conflicts of interest to declare.

Acknowledgement

The authors are grateful to the Research Council of Norway, through 1) its Centers of Excellence funding scheme, project number 262644, PoreLab (DB and SK) and 2) HighEff, a Centre for Environment-friendly Energy Research, project number 257632 (EM). CC is grateful for support from Department of Chemistry, Norwegian University of Science and Technology and to the Facultad de Ciencias of Universidad Nacional de Colombia Sede Medellin for partial supporting under the grant QUIPU 201010021328.

7 Appendix A: Nomenclature, symbols and units

A Appendix B: Expressions for transport coefficients

The heats of transfer q_j^* per component are given by:

$$q_1^* = -\kappa \Delta H_1 \tag{42}$$

$$q_1^* = -\kappa\, C_{p,CO}(T^g - T_{\mathrm{ref}}) \tag{43}$$

$$q_1^* = -2.1 \times 10^5 \mathrm{J/kg} \tag{44}$$

View Article Online
DOI: 10.1039/C9CP02389E

$$q_2^* = -\kappa \Delta H_2 \tag{45}$$

$$q_2^* = -\kappa\, C_{p,O_2}(T^g - T_{\text{ref}}) \tag{46}$$

$$q_2^* = -1.9 \times 10^5 \text{J/kg} \tag{47}$$

where $T_{\text{ref}} = 298\text{K}$ and $C_{p,j}$ is the heat capacity of component j.

Now, we check whether the following relations are fulfilled:

$$\left(r_{\text{rq}}^{\text{s,g}}\right)^2 \leq r_{\text{qq}}^{\text{s,g}}\, r_{\text{rr}}^{\text{s,g}}$$

$$1.8 \times 10^{12} \leq 7.3 \times 10^{13}$$

$$\left(r_{\text{q1}}^{\text{s,g}}\right)^2 \leq r_{\text{qq}}^{\text{s,g}}\, r_{11}^{\text{s,g}}$$

$$1.3 \times 10^{-1} \leq 3.7 \times 10^{5}$$

$$\left(r_{\text{q2}}^{\text{s,g}}\right)^2 \leq r_{\text{qq}}^{\text{s,g}}\, r_{22}^{\text{s,g}}$$

$$1.1 \times 10^{-8} \leq 3.3 \times 10^{5}$$

It is important to note that H_j^0 and S_j^0 are used to calculate the chemical potentials in the gas phase, as follows:

$$\mu_j = \mu_j^0 + RT \ln(x_j)$$

where

$$\mu_j^0 = H_j + T\, S_j$$

The partial molar enthalpy, H_j, and the partial molar entropy,S_j, are given by:

$$H_j = H_j^0 + \Delta T C_p$$

$$S_j = S_j^0 + C_p\, ln\left(\frac{T}{T_{ref}}\right)$$

where $\Delta T = T - T_{\text{ref}}$ and $T_{\text{ref}} = 273\ K$. The reaction Gibbs energy is calculated from the chemical potentials

$$\Delta_r G^s = \sum_{j=1}^{n} \nu_j \mu_j$$

where ν_j is the stoichiometric coefficient.

$$\Delta_r G^s = \mu_{CO_2}^s - \frac{1}{2}\mu_{O_2}^s - \mu_{CO}^s$$

Notes and references

1 I. Chorkendorff and J. W. Niemantsverdriet, *Concepts of modern catalysis and kinetics*, John Wiley & Sons, 2006.

2 J. J. Carberry, *Ind. Eng. Chem. Fundamen.*, 1975, **14**, 129–131.

3 P. Kočí, F. Štěpánek, M. Kubíček and M. Marek, *Chem. Eng. Sci.*, 2007, **62**, 5380–5385.

4 F. E. Genceli, M. Rodriguez Pascual, S. Kjelstrup and G.-J. Witkamp, *Crystal Growth and Design*, 2009, **9**, 1318–1326.

5 F. E. G. G"uner, J. Wåhlin, M. Hinge and S. Kjelstrup, *Chemical Physics Letters*, 2015, **622**, 15–19.

6 V. Badam, V. Kumar, F. Durst and K. Danov, *Experimental Thermal and Fluid Science*, 2007, **32**, 276–292.

7 W. L. Perry, D. W. Cooke, J. D. Katz and A. K. Datye, *Catal. Letters*, 1997, **47**, 1–4.

8 W. L. Perry, J. D. Katz, D. Rees, M. T. Paffet and A. K. Datye, *Journal of Catalysis*, 1997, **171**, 431–438.

9 M. Suzuki, V. Tseeb, K. Oyama and S. Ishiwata, *Biophysical journal*, 2007, **92**, L46–L48.

10 G. C. Bond, M. A. Keane, H. Kral and J. A. Lercher, *Cat. Rev.-Sci. Eng.*, 2000, **42**, 323–383.

11 S. Vyazovkin, *New J. Chem.*, 2000, **24**, 913–917.

12 Ø. Wilhelmsen, D. Bedeaux, S. Kjelstrup and D. Reguera, *Adv. Nat. Sci.: Nanosci. Nanotech.*, 2014, **5**, 015009.

13 D. Bedeaux, S. Kjelstrup, L. Zhu and G. J. M. Koper, *Phys. Chem. Chem. Phys.*, 2006, **8**, 5421–5427.

14 S. Kjelstrup and D. Bedeaux, *Non-equilibrium thermodynamics of heterogeneous systems*, World Scientific, 2008, vol. 16.

15 L. Zhu and G. Frens, *J. Phys. Chem. B*, 2006, **110**, 18307–18312.

16 A. Lervik, S. Kjelstrup and H. Qian, *Phys. Chem. Chem. Phys.*, 2015, **17**, 1317–1324.

17 L. D. Meis and A. L. Vianna, *Annu. Rev. Biochem.*, 1979, **48**, 275–292.

18 S. Kjelstrup, L. De Meis, D. Bedeaux and J.-M. Simon, *Eur. Biophys. J.*, 2008, **38**, 59–67.

19 D. Bedeaux and S. Kjelstrup, *Phys. Chem. Chem. Phys.*, 2008, **10**, 7304–7317.

20 T. Engel and G. Ertl, *Adv. Catal.*, Elsevier, 1979, vol. 28, pp. 1–78.

21 C. Campbell, G. Ertl, H. Kuipers and J. Segner, *Surf. Sci.*, 1981, **107**, 207–219.

22 R. Baxter and P. Hu, *J. Chem. Phys.*, 2002, **116**, 4379–4381.

23 L. Onsager, *Phys. Rev.*, 1931, **37**, 405.

24 L. Onsager, *Phys. Rev.*, 1931, **38**, 2265.

25 E. Magnanelli, Ø. Wilhelmsen, E. Johannessen and S. Kjelstrup, *J. Memb. Sci.*, 2016, **513**, 129–139.

26 R. Skorpa, M. Voldsund, M. Takla, S. K. Schnell, D. Bedeaux and S. Kjelstrup, *J. Memb. Sci.*, 2012, **394-395**, 131–139.

27 W. M. Deen, *Analysis of Transport Phenomena, Topics in Chemical Engineering*, Oxford University Press, New York, 1998, vol. 3.

28 R. Imbihl and G. Ertl, *Chem. Rev.*, 1995, **95**, 697–733.

29 R. H. Nibbelke, A. J. Nievergeld, J. H. Hoebink and G. B. Marin, *Appl. Catal. B*, 1998, **19**, 245–259.

30 S. Kjelstrup, D. Bedeaux, E. Johannessen and J. Gross, *Non-equilibrium thermodynamics for engineers*, World Scientific Publishing Co Inc, 2010.

View Article Online
DOI: 10.1039/C9CP02389E

31 Ø. Wilhelmsen, T. T. Trinh, S. Kjelstrup and D. Bedeaux, *J. Phys. Chem. C*, 2015, **119**, 8160–8173.

32 Ø. Wilhelmsen, T. T. Trinh, A. Lervik, V. K. Badam, S. Kjelstrup and D. Bedeaux, *Phys. Rev. E*, 2016, **93**, 032801.

33 *MATLAB Optimization Toolbox*, 2016b, The MathWorks, Natick, MA, USA.

34 L. F. Shampine and M. W. Reichelt, *SIAM J. Sci. Comput.*, 1997, **18**, 1–22.

35 E. N. Fuller, P. D. Schettler and J. C. Giddings, *Ind. Eng. Chem.*, 1966, **16**, 551.

36 Y. Yeo, L. Vattuone and D. King, *J. Chem. Phys.*, 1997, **106**, 392–401.

37 I. Barin and G. Platzki, *Thermochemical data of pure substances*, Wiley Online Library, 1989, vol. 304.

38 N. B. Vargaftik, *Handbook of physical properties of liquids and gases-pure substances and mixtures*, Hemisphere Publishing Corporation, New York, NY, 1975.

39 G. Grimvall, *Thermophysical properties of materials*, Elsevier, 1999.

40 R. Taylor and R. Krishna, *Multicomponent Mass Transfer*, 1995, vol. 60, pp. 177–179.

41 M. V. Twigg, *Applied Catalysis B: Environmental*, 2007, **70**, 2–15.

42 L. Zhu, G. J. Koper and D. Bedeaux, *J. Phys. Chem. A*, 2006, **110**, 4080–4088.

43 E. Johannessen and S. Kjelstrup, *Chem. Eng. Sci.*, 2005, **60**, 3347–3361.

View Article Online
DOI: 10.1039/C9CP02389E

Table 2 Parameters and system properties used in the simulations.

Property-Parameter	Value	Units	Reference
p	1×10^5	Pa	
R	8.314	J mol^{-1} K^{-1}	
$C_{0,\mathrm{CO}}$	12.2	mol m^{-3}	
$C_{0,\mathrm{O_2}}$	12.2	mol m^{-3}	
$C_{0,\mathrm{CO_2}}$	6.1	mol m^{-3}	
$C^{\mathrm{s}}_{\mathrm{CO}}$	9.7×10^{-4}	mol kg$^{-1}_{\mathrm{cat}}$	
$C^{\mathrm{s}}_{\mathrm{O_2}}$	9.7×10^{-4}	mol kg$^{-1}_{\mathrm{cat}}$	
$C^{\mathrm{s}}_{\mathrm{CO_2}}$	8.5×10^{-3}	mol kg$^{-1}_{\mathrm{cat}}$	
$D^{\mathrm{g}}_{\mathrm{CO}}$	3.4×10^{-5}	m^2 s^{-1}	27,35
$D^{\mathrm{g}}_{\mathrm{O_2}}$	2.8×10^{-5}	m^2 s^{-1}	27,35
$D^{\mathrm{g}}_{\mathrm{CO_2}}$	3.1×10^{-5}	m^2 s^{-1}	27,35
$k_{\mathrm{f,CO}}$	3×10^6	mol Pa^{-1}kg$^{-1}_{\mathrm{cat}}$ s^{-1}	20,28
$k_{\mathrm{b,CO}}$	2×10^{16}	s^{-1}	20,28
$k_{\mathrm{f,O_2}}$	2.3×10^7	Pa s^{-1}	
k_{f}	1.2×10^{-6}	kg$_{\mathrm{cat}}$ mol^{-1} s^{-1}	
k_{b}	1.2×10^{-16}	kg$_{\mathrm{cat}}$ mol^{-1} s^{-1}	
$E_{\mathrm{a,b,CO}}$	159	kJ mol^{-1}	20,28
$E_{\mathrm{a,f}}$	72	kJ mol^{-1}	20,21
K_{CO}	3.6×10^{11}	-	20
$K_{\mathrm{O_2}}$	2.3×10^7	-	20
$\Delta H^{\mathrm{s,g}}_{\mathrm{CO}}$	180	kJ mol^{-1}	36
$\Delta H^{\mathrm{s,g}}_{\mathrm{O_2}}$	340	kJ mol^{-1}	36
H^0_{CO}	-110.5	kJ mol^{-1}	37
S^0_{CO}	197.6	J mol^{-1} K^{-1}	37
$S^0_{\mathrm{O_2}}$	205.0	J mol^{-1} K^{-1}	37
δ^{s}	1×10^{-9}	m	
δ^{g}	1×10^{-4}	m	
δ^{c}	1×10^{-4}	m	
λ^{g}	0.0232	W m^{-1}K^{-1}	38,39
λ^{c}	72	W m^{-1}K^{-1}	39
ρ^{c}	719	kg m^{-3}	38

View Article Online
DOI: 10.1039/C9CP02389E

Table A.1 Symbols of properties and parameters

Property-Parameter	Symbol	Units
Heat capacity	C_p	J mol^{-1} K^{-1}
Pressure	p	Pa
Temperature	$T, T^{\mathrm{g}}, T^{\mathrm{s}}, T^{\mathrm{c}}$	K
Molar fraction of component j	x_j	-
Gas constant	R	J mol^{-1} K^{-1}
Total heat flux	J_{q}	W m^{-2}
Measurable heat flux	J'_{q}	W m^{-2}
Molar flux of the component j	J_j	mol s^{-1} m^{-2}
Chemical potential	μ_j	J mol^{-1}
Partial molar enthalpy of component j	H_j	J mol^{-1}
Thermal conductivity	λ	W m^{-1} K^{-1}
Diffusion coefficient of component j	D_j	m^2 s^{-1}
Concentration of component j in the gas	C_j	mol m^{-3}
Concentration of component j at the surface	C_j^{s}	mol kg$_{cat}^{-1}$
Reaction Gibbs energy	$\Delta_{\mathrm{r}}G^{\mathrm{s}}$	kJ mol^{-1}
Adsorption Entalphy of component j	$\Delta H_j^{\mathrm{s,g}}$	kJ mol^{-1}
Reaction rate	ν	mol kg$_{cat}^{-1}$ s^{-1}
Pre-exponential factor	k_0	
Activation energy	E_{a}	kJ mol^{-1}
Equilibrium constant	K	
Forward kinetic constant	k_{f}	kg$_{cat}$ mol^{-1} s^{-1}
Backward kinetic constant	k_{b}	kg$_{cat}$ mol^{-1} s^{-1}
Heat of transfer	q_j^*	J mol^{-1}

View Article Online
DOI: 10.1039/C9CP02389E

Table B.1 Equations of the transport coefficients at the surface

Coefficient	Symbol	Expression
Heat transfer in the gas film	r^{g}_{qq}	$\frac{1}{\lambda^{g}(T^{g})^2}$
Mass transfer in the gas film	r^{g}_{jj}	$\frac{1}{D_j T^{g}} \frac{\partial \mu_j}{\partial C_j}\Big\vert_{x=0}$
Heat transfer at the surface	$r^{\mathrm{s,g}}_{\mathrm{qq}}$	$\beta \delta^{\mathrm{s}} r^{g}_{\mathrm{qq}}$
Heat transfer at the surface	$r^{\mathrm{s,c}}_{\mathrm{qq}}$	$\beta \delta^{\mathrm{s}} \frac{1}{\lambda^{\mathrm{c}}(T^{\mathrm{c}})^2}$
Mass transfer at the surface	$r^{\mathrm{s,g}}_{jj}$	$\beta \delta^{\mathrm{s}} r^{g}_{jj}$
Coupling heat-mass transfer	$r^{\mathrm{s,g}}_{\mathrm{q}j}$	$-r^{\mathrm{s,g}}_{\mathrm{qq}} q^{*}_{j}$
Surface Mass transfer	$r^{\mathrm{s,g}}_{jj}$	$\frac{-\Delta G^{\mathrm{s,g}}_{j}\vert_{T=\mathrm{const.}}}{T \nu_j}$
Coupling heat transfer-reaction	$r^{\mathrm{s,g}}_{\mathrm{rq}}$	$\sqrt{\alpha\, r^{\mathrm{s,g}}_{\mathrm{qq}} r^{\mathrm{s,g}}_{\mathrm{rr}}}$
Chemical reaction	$r^{\mathrm{s}}_{\mathrm{rr}}$	$[1-\exp(\frac{\Delta_{\mathrm{r}} G^{\mathrm{s}}}{R T^{\mathrm{s}}})]/\nu^{\mathrm{s}}$

Table B.2 Main coefficient and coupling coefficient of the surface at $T^{s} = 500$ K and inlet mole fraction of the gases. The scaling factors are $\beta = 10^{6}$, $\kappa = 1$ and $\alpha = 0.9$.

Coefficient	Value	Unit
$r^{\mathrm{s,g}}_{\mathrm{qq}}$	$\beta\delta r^{g}_{\mathrm{qq}} = \frac{\beta\delta}{\lambda^{g} T^2} = 1.7\times10^{-7}$	$\mathrm{m^2\ s\ J^{-1}\ K^{-1}}$
$r^{\mathrm{s,c}}_{\mathrm{qq}}$	$\beta\delta r^{c}_{\mathrm{qq}} = \frac{\beta\delta}{\lambda^{c} T^2} = 5.6\times10^{-11}$	$\mathrm{m^2\ s\ J^{-1}\ K^{-1}}$
$r^{\mathrm{s,g}}_{\mathrm{q1}}$	$-r^{s,g}_{qq} q^{*}_{1} = 3.6\times10^{-1}$	$\mathrm{m^2\ s\ kg^{-1}\ K^{-1}}$
$r^{\mathrm{s,g}}_{\mathrm{q2}}$	$-r^{s,g}_{qq} q^{*}_{2} = 1.0\times10^{-4}$	$\mathrm{m^2\ s\ kg^{-1}\ K^{-1}}$
$r^{\mathrm{s,g}}_{11}$	$-\frac{1}{\nu_{\mathrm{CO}}} \frac{\Delta G^{\mathrm{s,g}}_{\mathrm{CO}}\vert_{J^{g}_{\mathrm{q}}=0}}{T} = 2.2\times10^{11}$	$\mathrm{J\ s\ m^2\ K^{-1}\ kg^{-2}}$
$r^{\mathrm{s,g}}_{22}$	$-\frac{1}{\nu_{\mathrm{O_2}}} \frac{\Delta G^{\mathrm{s,g}}_{\mathrm{O_2}}\vert_{J^{g}_{\mathrm{q}}=0}}{T} = 2.0\times10^{11}$	$\mathrm{J\ s\ m^2\ K^{-1}\ kg^{-2}}$
$r^{\mathrm{s,g}}_{\mathrm{rq}}$	$\sqrt{\alpha r^{\mathrm{s,g}}_{\mathrm{qq}} r^{\mathrm{s,g}}_{\mathrm{rr}}} = 1.4\times10^{6}$	$\mathrm{m^2\ W^{-1}}$
$r^{\mathrm{s}}_{\mathrm{rr}}$	$\frac{1}{\nu^{s}}\left[1-\exp\left(\frac{\Delta_{\mathrm{r}} G^{\mathrm{s}}}{R T^{\mathrm{s}}}\right)\right] = 4.3\times10^{19}$	$\mathrm{s\ kg_{cat}\ kg_{CO}^{-1}}$

Table B.3 Heat capacity of reactants: carbon monoxide and oxygen

C_p	Value	Unit
$C_{p,CO}$	1.0×10^{3}	$\mathrm{J\ kg^{-1}\ K^{-1}}$
C_{p,O_2}	9.2×10^{2}	$\mathrm{J\ kg^{-1}\ K^{-1}}$